http://dx.doi.org/10.5012/bkcs.2013.34.11.3335

Temperature-dependent Photoluminescence of Boron-doped ZnO Nanorods

Soaram Kim, Hyunggil Park, Giwoong Nam, Hyunsik Yoon, Jong Su Kim,[†] Jin Soo Kim,[‡] Jeong-Sik Son,[§] Sang-heon Lee,[#] and Jae-Young Leem[*]

Department of Nano Systems Engineering, Center for Nano Manufacturing, Inje University, Gimhae, Gyungnam 621-749, Korea
[*]E-mail: jyleem@inje.ac.kr
[†]Department of Physics, Yeungnam University, Gyeongsan, Gyeongbuk 712-749, Korea
[‡]Research Center of Advanced Materials Development (RCAMD), Division of Advanced Materials Engineering, Chonbuk National University, Jeonju, Chonbuk 561-756, Korea
[§]Department of Visual Optics, Kyungwoon University, Gumi, Gyeongbuk 730-850, Korea
[#]School of Chemical Engineering, Yeungnam University, Gyeongsan 712-749, Korea
Received July 4, 2013, Accepted August 25, 2013

Boron-doped ZnO (BZO) nanorods were grown on quartz substrates using hydrothermal synthesis, and the temperature-dependence of their photoluminescence (PL) was measured in order to investigate the origins of their PL properties. In the UV range, near-band-edge emission (NBE) was observed from 3.1 to 3.4 eV; this was attributed to various transitions including recombination of free excitons and their longitudinal optical (LO) phonon replicas, and donor-acceptor pair (DAP) recombination, depending on the local lattice configuration and the presence of defects. At a temperature of 12 K, the NBE produces seven peaks at 3.386, 3.368, 3.337, 3.296, 3.258, 3.184, and 3.106 eV. These peaks are, respectively, assigned to free excitons (FX), neutral-donor bound excitons (D^oX), and the first LO phonon replicas of D^oX, DAP, DAP-1LO, DAP-2LO, and DAP-3LO. The peak position of the FX and DAP were also fitted to Varshni's empirical formula for the variation in the band gap energy with temperature. The activation energy of FX was about ~70 meV, while that of DAP was about ~38 meV. We also discuss the low temperature PL near 2.251 eV, related to structural defects.

Key Words : Zinc oxide, B-doped, Hydrothermal, Nanorods, Photoluminescence

Introduction

Zinc oxide (ZnO) has potential applications in opto-electronic devices[1] and spintronics[2] because of its unique properties, such as a wide band gap (3.37 eV) and high exciton binding energy (60 meV) at room temperature (RT).[3] Many efforts to grow ZnO thin films on various substrates have been a focus for some time as a route to overcome the lattice mismatch between different substrates and ZnO. Nevertheless, the lattice mismatch hinders the possibility of defect free growth of ZnO thin films heterostructres. In general, ZnO has a strong tendency for selforganized growth and therefore this important property has led to grow ZnO nanostructures.[1] Among ZnO nanostructures, one-dimensional (1D) nanorods have been the focus of current research in physics, chemistry, and materials science due to their fundamental research significance as well as their technological applications.[4] In addition, ZnO nanorods has more advantage for LEDs and would be the integration of n-ZnO nanorods on other p-type substrates due to the fact that nanorods of ZnO have no need for a lattice matched substrate for the overgrowth compared to ZnO thin films.[5] The n-type doping of ZnO nanorods is necessary in order to fabricate electronic and optoelectronic devices and to enhance device performance, because n-type doping with Group III elements yields high-conductivity ZnO nanorods more easily compared to p-type doping. Other authors have reported 1D ZnO nanorods that are B-doped,[6,7] Al-doped,[8,9] Ga-doped,[10,11] and In-doped.[12,13] However, relative to the amount of literature available on other types of doping, there are few published reports to date on the properties of B-doped ZnO (BZO), although BZO can be used as dye-sensitized solar cells and as the transparent electrode in optoelectronic devices.[6,7] In our previous study,[14] we demonstrated the hydrothermal synthesis of BZO nanorods and found that this method allows the level of B-doping to be easily adjusted to tune the optical and electrical properties of ZnO nanorods according to the needs of various applications. Thus, we herein focus on the temperature-dependent photoluminescence (PL) of BZO nanorods in order to elucidate their optical properties. Low-temperature PL is a very sensitive tool for characterizing donor impurities and understanding the optical properties of materials.

Experimental

Sol-gel spin-coating was used to deposit ZnO seed layers onto quartz substrates. Zinc acetate dihydrate ($[Zn(CH_3COO)_2{\cdot}2H_2O]$, Sigma-Aldrich, purity 99%) was used as a starting material. Monoethanolamine (MEA, $[C_2H_7NO]$, Sigma-Aldrich, purity 99%) was used as the stabilizer, and 2-methoxyethanol ($[CH_3OCH_2CH_2OH]$, Sigma-

Aldrich, purity 99.5%) was used as the solvent. The molar ratio of zinc acetate to MEA was 1:1. The stabilized sol solution was stirred at 60 °C for 2 h to produce a clear, homogeneous solution that was subsequently aged at room temperature for 24 h. The aged sol solution was spin-coated for 20 s onto quartz substrates rotating at 3000 rpm to produce ZnO seed layers that were subsequently pre-heated at 300 °C for 10 min to evaporate the solvent and remove any residual organic material. The preheated ZnO seed layers were cooled at 5 °C/min to prevent the formation of cracks. The ZnO seed layers were coated, pre-heated, and cooled three times each and were then post-heated in a furnace at 550 °C in air for 1 h.

The BZO nanorods were then hydrothermally grown on the postheated ZnO seed layers. The ZnO seed layers were transferred to a Teflon-lined autoclave containing an aqueous solution of 0.1 M zinc nitrate hexahydrate ($[Zn(NO_3)_2 \cdot 6H_2O]$, Sigma-Aldrich 99%) hexamethylenetetramine (HMT, $[(CH_2)_6N_4]$, Sigma-Aldrich) and triisopropyl borate ($[((CH_3)_2CHO)_3B]$, Sigma-Aldrich 98%). The concentration of boron in the aqueous solution was adjusted to provide a doping concentration of B/Zn = 2.5 at.%. The nanorods were hydrothermally grown in an autoclave at 95 °C for 4 h. After the reaction had completed, the hydrothermally grown nanorods were rinsed with deionized water and blow-dried with ultra-high-purity (99.9999%) nitrogen to remove any unreacted residual salts and organic materials. The top-view of the BZO nanorods was observed by field emission scanning electron microscopy (FE-SEM). optical properties of the hydrothermally grown ZnO nanorods doped with 2.5 at.% B were investigated using PL. Their spectra were measured at RT, low temperature (12 K), and over a range of temperatures, using a He-Cd laser (325 nm, 2.55 W/cm^2) as the excitation source and a 0.75-m single-grating monochromator equipped with a photomultiplier tube as the detector.

Results and Discussion

Figure 1(a) shows the PL spectrum of the BZO nanorods at 300 K, with typical emission in the UV and visible range. The inset shows the top-view SEM image of ZnO nanorods. The BZO nanorods had grown well on the ZnO seed layers and were hexagonal. The strong UV emission from 3.1 to 3.4 eV, which corresponds to near-band-edge emission (NBE), is attributed to various transitions including recombination of free excitons (FX) and its longitudinal optical (LO)-phonon replicas,[15,16] free-to-neutral acceptor (FA) transitions,[17] and donor-acceptor pair (DAP) recombination,[18,19] depending on the local lattice configuration and the presence of defects.[20] In addition, broad deep-level emission (DLE) occurs at 2.251 eV (green emission) in the visible region; DLE is usually attributed to structural defects such as Zn vacancies (V_{Zn})[21] and singly ionized oxygen vacancies (V_O^+)[22] in the ZnO crystal lattice. In general, the luminescence of ZnO nanorods shows higher intensity of DLE and various their origins compared to ZnO thin films.[23-25] Thus, the undoped and doped ZnO thin films does not give much insight into detailed impurity related recombination processes as demonstrated in luminescence.[26,27] Interestingly, there was a shoulder at about 3.3 eV in the NBE; a low-temperature PL spectrum was obtained to further confirm the origin of this peak for BZO nanorods Figure 1(b) shows the PL spectrum of the BZO nanorods at 12 K in the UV region. Further analyses have revealed that all spectra can be well fitted by Gaussian function. There are seven peaks at 3.386, 3.368, 3.337, 3.296, 3.258, 3.184, and 3.106 eV. It is plausible that the reason for the difference of energy is due to different origin in the BZO nanorods although it comes from the same sample. The peak at 3.386 eV was tentatively attributed to FX recombination, and the peak at 3.368 eV and 3.296 eV were assigned to the neutral-donor bound exciton (D^oX) recombination and first LO phonon replicas of D^oX.[28,29] In addition, the peaks in the region between 3.337 and 3.106 eV were assigned as DAP transitions and LO phonon replicas of DAP. The energy spacings between the D^oX and D^oX-1LO, the DAP and DAP-1LO, the DAP-1LO and DAP-2LO, and the DAP-2LO and DAP-3LO were 72, 79, 74, and 78 meV, respectively, which agrees approximately with the reported energy of the

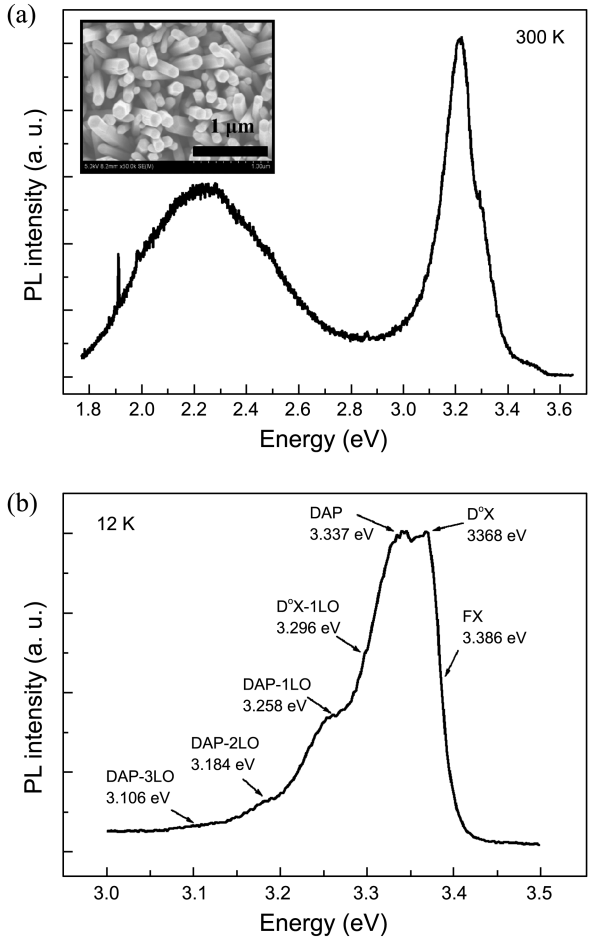

Figure 1. PL spectrum of BZO nanorods at (a) 300 K and the inset shows the top-view SEM image of ZnO nanorods. (b) PL spectrum of the BZO nanorods at 12 K in the UV region.

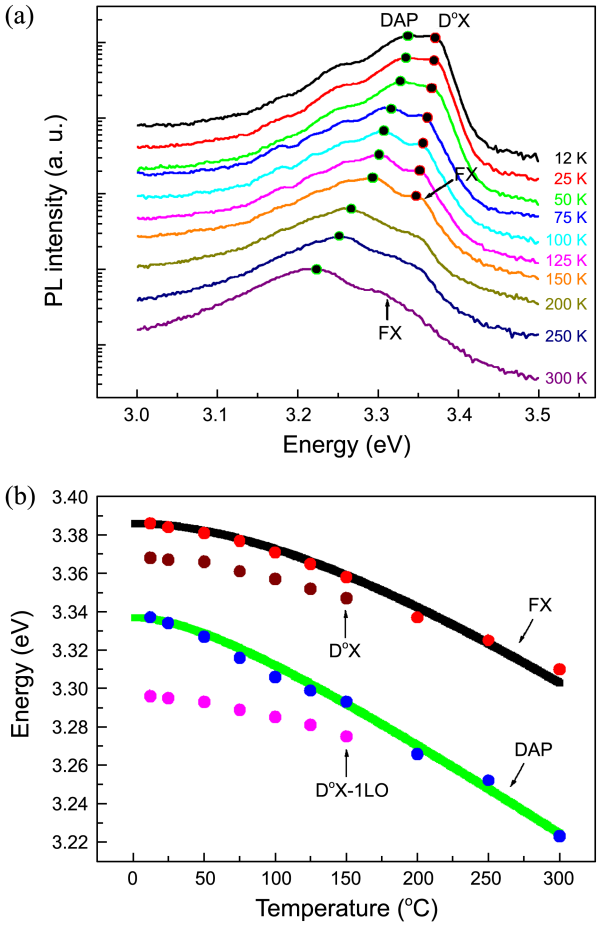

Figure 2. (a) Temperature-dependent PL spectra of BZO nanorods ranging from 12 to 300 K, exhibiting NBE. (b) Positions of D°X and DAP PL peaks as a function of temperature.

LO-phonon ($\hbar\omega_{LO} = 72$ meV).[30,31] In general, these pronounced replicas originate from strong exciton-phonon coupling effect due to the high ionicity and polarity of ZnO.[31-33]

Figure 2(a) shows the temperature-dependent PL spectra of the BZO nanorods measured in the temperature range 12-300 K. The position of the PL peaks shifted with increasing temperature, and their intensity gradually decreased. In general, as the temperature increases, the interaction between FX and D°X becomes weaker, until finally the D°X are freed, that is, increasing the temperature raises the probability that the bound excitons will be ionized and eventually become free excitons.[28] Thus, the intensity of the D°X emission was drastically decreased in comparison with that of the FX emission; the transition of the FX becomes dominant at high temperature. This trend is illustrated by the smaller FX peak, which appears at 150 K and, at 200 K becomes higher than the D°X peak, as shown in Figure 2(a). In addition, the D°X peaks shifted to lower energy (red-shift) with increasing temperature. This is because the thermal energy protects the exciton localization energy, and the line shape of the emission peak adopts the characteristic line shape of FX recombination, leading to a red-shift characteristic of the temperature-dependence of the band-gap energy.[29]

On the other hand, the D°X-1LO gradually merges into the DAP transition as the temperature increases, broadening the NBE emission. Also, the DAP transition remains at higher temperature compared to D°X, consistent with a previous report by Chen *et al.*[28] which stated that the DAP transition indicates that the impurities involved have larger binding energies and thus require higher thermal energy to become ionized. In addition, it is well established that at higher temperature, the DAP transition will transform to recombination between free electrons and acceptors (eA°); this process is associated with an energy slightly higher than that of DAP, due to the ionization of electrons bound to neutral donors.[34-36] Hence, the broad NBE peak at 3.223 eV results from the merging of all the PL bands when the temperature is increased to RT. Also, the peaks of the DAP transition shifted to the lower energy region (red-shift) with increasing temperature, which can thus be easily understood by using the Eq. (1) for the energy of a DAP emission:[37]

$$E_{DAP} = E_g - E_a - E_d + \frac{e^2}{4\pi\varepsilon_0\varepsilon r_{da}}, \quad (1)$$

where E_g is the band gap energy while E_a and E_d are the acceptor and donor binding energies, respectively. The last term of the equation represents the Coulomb interaction energy between the donor and the acceptor, and r_{da} refers to the average DAP distance. Thus, a higher temperature increases the average donor-acceptor distance, thereby decreasing the Coulomb energy term and leading to a red-shift of the DAP peak. Figure 2(b) shows the variation of the PL peak energies of the BZO nanorods as a function of temperature. Also, the peak position of the FX and DAP were fitted to Varshni's empirical formula for the variation in the band gap energy with temperature:[38]

$$E_g(T) = E_g(0) - \frac{\alpha T^2}{\beta + T}, \quad (2)$$

where $E_g(T)$ is the band gap at an absolute temperature T and α and β are the Varshini thermal coefficients related with ZnO. The solid line shown in Figure 2(b) denotes the fitting of the data to Eq. (2) for the FX and DAP transition from 12 to 300 K. The obtained fitting parameters of E_g, α, and β for FX were 3.386 eV, 6×10^{-4} eV/K, and 350 K, while those for the DAP transition were 3.337 eV, 5×10^{-4} eV/K, and 100 K, respectively.

Figure 3(a) and (b) shows the integrated PL intensity of the FX and DAP transition in BZO nanorods as a function of temperature from 12 to 300 K. In general, the temperature-dependent integrated PL intensity can be described by the following dual activation energy model:[39]

$$I(T) = \frac{I(0)}{[1 + c_1 \exp(-E_{a1}/kT) + c_2 \exp(-E_{a2}/kT)]}, \quad (3)$$

where E_{a1} and E_{a2} denote the activation energies for two different thermal activation processes, and the parameters c_1 and c_2 are the relative ratios of nonradiative recombination and reflect the competition between the recapture and the nonradiative recombination. And k is the Boltzman

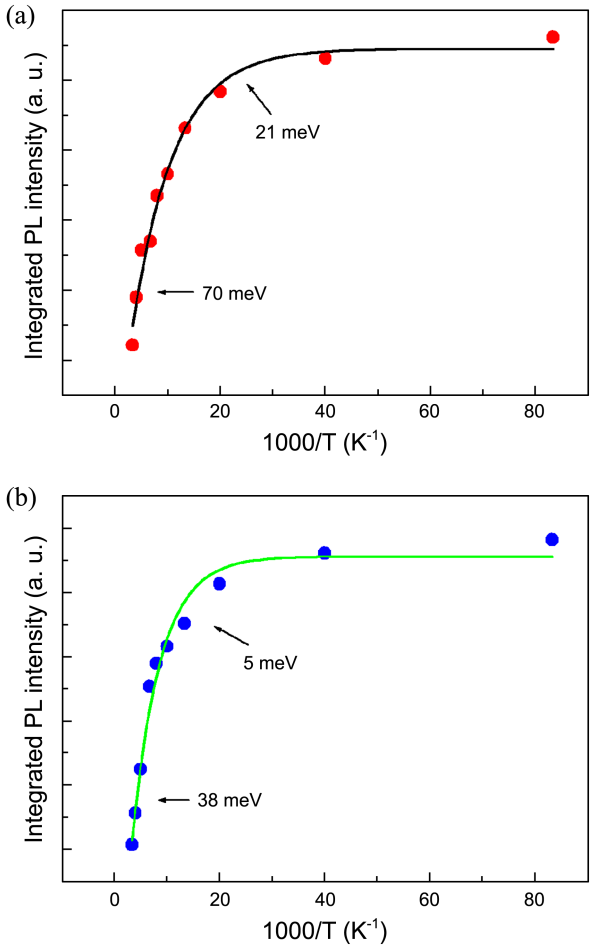

Figure 3. Integrated PL intensities of the (a) D°X and (b) DAP transitions in BZO nanorods over the temperature range from 12 to 300 K.

constant, T is temperature. Thus, in this experession, the presence of two E_a accounts for two competitive non-radiative recombination channels. The curve fit gives rise to activation energies of 70 and 21 meV for FX, and 38 and 5 meV for DAP. The activation energies of 70 and 21 meV may represent the thermal ionization energies of the BZO nanorods. However, the DAP transition comprises the radiative combination of electrons on the neutral donors with holes on the neutral acceptors. It is well known that the defect binding energy falls in the range of 5-50 meV for donors and 20-200 meV for acceptors, depending on the material parameters.[40] Thus, we guess that the thermal activation energy of 5 meV is the donor binding energy, while the 38 meV activation energy is the acceptor binding energy.

Conclusions

BZO nanorods were grown by hydrothermal synthesis, and their temperature-dependent PL, which occurs primarily in the UV range, was investigated. The PL emission mechanisms of BZO nanorods, and the variations in these mechanisms with temperature, were discussed. The low-temperature PL spectrum of the BZO nanorods showed features characteristic of FX, D°X, DAP, and their relevant LO-phonon replicas. Increasing the temperature resulted in a red-shift of the emission energies. The PL emission energies were fitted numerically using Varshni's empirical formula for the variation in the band gap with temperature. The values of Varshni's empirical formula fitting parameters were $E_g = 3.386$, $\alpha = 6 \times 10^{-4}$ eV/K, and $\beta = 350$ K for FX, and $E_g = 3.337$, $\alpha = 5 \times 10^{-4}$ eV/K, and $\beta = 100$ K for the DAP transition. In addition, all of the activation energies were estimated to be ~70 meV. Hence, our results indicate that BZO nanorods can help to advance photonic and opto-electronic devices.

Acknowledgments. This research was supported by Basic Science Research Program through the National Research Foundation of Korea (NRF) funded by the Ministry of Education, Science and Technology (No. 2012R1A1B3001837).

References

1. Willander, M.; Nur, O.; Zhao, Q. X.; Yang, L. L.; Lorenz, M.; Cao, B. Q.; Pérez, J. Z.; Czekalla, C.; Zimmermann, G.; Grundmann, M.; Bakin, A.; Behrends, A.; Suleiman, M. A.; Shaer, A. E.; Mofor, A. C.; Postels, B.; Waag, A.; Boukos, N.; Trvalos, A.; Kwack, H. S.; Guinard, J.; Dang, D. L. S. *Nonotechnology* **2009**, *20*, 332001.
2. Pearton, S. J.; Norton, D. P.; Heo, Y. W.; Tien, L. C.; Ivill, M. P.; Li, Y.; Kang, B. S.; Ren, F.; Kelly, J.; Hebard, A. F. *J. Electron. Mater.* **2006**, *35*, 862.
3. Kim, S.; Kim, M. S.; Yim, K. G.; Nam, G.; Lee, D.-Y.; Kim, J. S.; Kim, J. S.; Son, J.-S.; Leem, J.-Y. *J. Korean Phys. Soc.* **2012**, *60*, 1599.
4. Xia, Y.; Yang, P.; Sun, Y.; Wu, Y.; Mayers, B.; Gates, B.; Yin, Y.; Kim, F.; Yan, H. *Adv. Mater.* **2003**, *15*, 353.
5. Willander, M.; Yang, L. L.; Wadeasa, A.; Ali, S. U.; Asif, M. H.; Zhao, Q. X.; Nur, O. *J. Mater. Chem.* **2009**, *19*, 1006.
6. Pawar, B. N.; Cai, G.; Ham, D.; Mane, R. S.; Ganesh, T.; Ghule, A.; Sharma, R.; Jadhava, K. D.; Han, S.-H. *Sol. Energ. Mat. Sol. C* **2009**, *93*, 524.
7. Steinhauser, J.; Fay, S.; Oliveria, N.; Vallat-Sauvain, E.; Ballif, C. *Appl. Phys. Lett.* **2007**, *90*, 142107.
8. Kim, S.; Kim, M. S.; Nam, G.; Leem, J.-Y. *Electron. Mater. Lett.* **2012**, *8*, 445.
9. Lu, W.-L.; Hung, P.-K.; Hung, C.-I.; Yeh, C.-H.; Houng, M.-P. *Mater. Chem. Phys.* **2011**, *130*, 619.
10. Zhu, L.; Li, J.; Ye, Z.; He, H.; Chen, X.; Zhao, B. *Opt. Mater,* **2008**, *31*, 237.
11. Pineda-Hernandez, G.; Escobedo-Morales, A.; Pal, U.; Chigo-Anota, E. *Mater. Chem. Phys.* **2012**, *135*, 810.
12. Kim, S.; Nam, G.; Park, H.; Yoon, H.; Lee, S.-H.; Kim, J. S.; Kim, J. S.; Kim, D. Y.; Kim, S.-O.; Leem, J.-Y. *Bull. Korean Chem. Soc.* **2013**, *34*, 1205.
13. Fang, T.-H.; Kang, S.-H. *Curr. Appl. Phys.* **2010**, *10*, 1076.
14. Kim, S.; Park, H.; Nam, G.; Yoon, H.; Kim, B.; Ji, I.; Kim, Y.; Kim, I.; Park, Y.; Kang, D.; Leem, J.-Y. *Electron. Mater. Lett.* (in press).
15. Wang, L.; Giles, N. C. *J. Appl. Phys.* **2003**, *94*, 973.
16. Makino, T.; Segawa, Y.; Yoshida, S.; Tsukazaki, A.; Ohtomo, A.; Kawasaki, M.; Koinuma, H. *J. Appl. Phys.* **2005**, *98*, 093520.
17. Zhang, B. P.; Binh, N. T.; Segawa, Y.; Kashiwaba, Y.; Haga, K. *Appl. Phys. Lett.* **2004**, *84*, 586.
18. Peng, W. Q.; Qu, S. C.; Cong, G. W.; Wang, Z. G. *Appl. Phys. Lett.* **2006**, *88*, 101902.
19. Yang, Z.; Liu, J. L. *J. Vac. Sci. Technol. B* **2010**, *28*(3), C3D6.

20. He, H. P.; Tang, H. P.; Ye, Z. Z.; Zhu, L. P.; Zhao, B. H.; Wang, L.; Li, X. H. *Appl. Phys. Lett.* **2007**, *90*, 023104.
21. Tuomisto, F.; Saarinen, K.; Look, D. C.; Farlow, G. C. *Phys. Rev. B* **2005**, *72*, 085206.
22. Djurisic, A. B.; Leung, Y. H.; Tam, K. H.; Ding, L.; Ge, W. K.; Chen, H. Y.; Gwo, S. *Appl. Phys. Lett.* **2006**, *88*, 103107.
23. Kim, S.; Nam, G.; Park, H.; Yoon, H.; Kim, M. S.; Kim, D. Y.; Kim, S.-O.; Leem, J. Y. *J. Nanosci. Nanotechnol.* **2013**, *13*, 6226.
24. Ting, C.-C.; Li, C.-H.; Kuo, C.-Y.; Hsu, C.-C.; Wang, H.-C.; Yang, M.-H. *Thin Solid Films* **2010**, *518*, 4156.
25. Lyu, S. C.; Zhang, Ye.; Ruh, H.; Lee, H.-J.; Shim, H-.W.; Suh, E.-K.; Lee, C. J. *Chem. Phys. Lett.* **2002**, *363*, 134.
26. Prezezdziecka, E.; Wachnicki, L.; Paszkowicz, W.; Lusakowska, E.; Krajewski, T.; Luka, G. Godlewski, M. *Semicond. Sci. Technol.* **2009**, *24*, 105014.
27. Nam, G.; Lee, S.-H.; So, W.; Yoon, H.; Park, H.; Kim, Y. G.; Kim, S.; Kim, M. S.; Jung, J. H.; Lee, J.; Kim, Y.; Leem, J.-Y. *Bull. Korean Chem. Soc.* **2013**, *34*, 95.
28. Chen, R.; Xing, G. Z.; Gao, J.; Zhang, Z.; Wu, T.; Sun, H. D. *Appl. Phys. Lett.* **2009**, *95*, 061908.
29. Nam, G.; Lee, S.-H.; Kim, S.; Kim, M. S.; Kim, D. Y.; Yim, K. G.; Lee, D.-Y.; Kim, J. S.; Kim, S. J.; Son, J.-S.; Kim, S.-O.; Jung, J. H.; Leem, J.-Y. *Jpn. J. Appl. Phys.* **2012**, *51*, 021102.
30. Reynolds, D. C.; Look, D. C.; Jogai, B. *J. Appl. Phys.* **2001**, *89*, 6189.
31. Hong, W.-K.; Jo, G.; Choe, M.; Lee, T.; Sohn, J. I.; Welland, M. E. *Appl. Phys. Lett.* **2009**, *94*, 043103.
32. Teke, A.; Ozgur, U.; Dogan, S.; Gu, X.; Morkoc, H.; Nemeth, B.; Nause, J.; Everitt, H. O. *Phys. Rev. B* **2004**, *70*, 195207.
33. Shan, W.; Walukiewicz, W.; Ager, J. W., III; Yu, K. M.; Yuan, H. B.; Xin, H. P.; Cantwell, G.; Song, J. J. *Appl. Phys. Lett.* **2005**, *86*, 191911.
34. Jie, J.; Wang, G.; Chen, Y.; Han, X.; Wang, Q.; Xu, B. *Appl. Phys. Lett.* **2005**, *86*, 031909.
35. Wang, L.; Giles, N. C. *Appl. Phys. Lett.* **2004**, *84*, 3049.
36. Zhang, B. P.; Binh, N. T.; Segawa, Y.; Wakatsuki, K.; Usami, N. *Appl. Phys. Lett.* **2003**, *83*, 1635.
37. Pankove, J. I. *Optical Processes in Semiconductors*; Prentice-Hall: Englewood Cliffs, New Jersey, 1971; p 143.
38. Varshini, Y. P. *Physica (Amsterdam)* **1967**, *34*, 149.
39. Leroux, M.; Grandjean, N.; Beaumont, B.; Nataf, G.; Semond, F.; Massies, J.; Gibart, P. *J. Appl. Phys.* **1999**, *86*, 3721.
40. Klingshirn, C. *Semiconductor Optics*; Springer: Berlin Heidelberg, 2004; p 222.